www.jmolecularsci.com

ISSN:1000-9035

# Antibacterial effects of an antibacterial drug-loaded chitosan-based nanoparticles

Priyanka Rathore <sup>1</sup>, Rishikesh Gupta <sup>1</sup>, Prem Prakash Singh <sup>1</sup>, and Alok Kumar Mahor\* <sup>1</sup> Institute of Pharmacy, Bundelkhand University <sup>1</sup>, Jhansi- 284128, Uttar Pradesh, India.

### Article Information

Received: 28-08-2025 Revised: 19-09-2025 Accepted: 22-10-2025 Published: 11-11-2025

### **Keywords**

Levofloxacin; Chitosan graphene oxide; Nanocomposite; Antimicrobial

resistance; Box–Behnken design; Wound therapy

#### **ABSTRACT**

The growing threat of antimicrobial resistance (AMR) necessitates the development of novel therapeutic strategies capable of restoring the efficacy of existing antibiotics. In this study, levofloxacin-loaded chitosangraphene oxide (CS-GO-LVX) nanocomposites were developed as a synergistic nanocarrier system to enhance antibacterial performance and drug stability. The nanocomposites were optimized using a Box-Behnken design, evaluating the effects of CS:GO ratio, glutaraldehyde concentration, stirring speed, and sonication time on key formulation parameters. The optimized formulation (CGLN4) exhibited a particle size of 209.9 nm, PDI of 0.22, and zeta potential of -33.2 mV, indicating uniformity and colloidal stability. FTIR confirmed strong electrostatic, hydrogen bonding, and Schiff base interactions among CS, GO, and LVX, ensuring structural integrity and sustained drug encapsulation. The optimized formulation achieved an entrapment efficiency of 85.3% and demonstrated pH-responsive sustained release (~85% over 18 h) following Fickian diffusion kinetics. SEM analysis revealed aggregated yet discrete nanosheets with rough morphology, consistent with nanoscale dispersion. Accelerated stability testing over six months showed acceptable physical and chemical stability, maintaining entrapment efficiency above 76%. The combined physicochemical and release characteristics indicate that CS-GO-LVX nanocomposites provide a stable and effective antibacterial platform with potential applications in combating resistant bacterial infections and promoting targeted dermal or wound drug delivery.

### ©2025 The authors

This is an Open Access article distributed under the terms of the Creative Commons Attribution (CC BY NC), which permits unrestricted use, distribution, and reproduction in any medium, as long as the original authors and source are cited. No permission is required from the authors or the publishers.(https://creativecommons.org/licenses/by-nc/4.0/)

### INTRODUCTION:

The escalating global crisis of antimicrobial resistance (AMR) poses one of the most significant threats to modern healthcare, with multidrugresistant bacterial infections contributing to millions of deaths annually and imposing substantial economic burdens on healthcare

systems worldwide [1,2]. The World Health Organization has identified antimicrobial resistance as one of the top ten global public health threats, necessitating urgent innovation in therapeutic strategies to combat resistant pathogens [3]. Traditional antibiotic monotherapy increasingly fails against evolving bacterial resistance mechanisms, driving the need for novel approaches that can enhance drug efficacy while potentially overcoming resistance barriers [4,5].

Levofloxacin (LVX), a third-generation fluoroquinolone antibiotic, demonstrates broad-spectrum activity against both Gram-positive and Gram-negative bacteria through inhibition of bacterial DNA gyrase and topoisomerase IV enzymes [6,7]. Levofloxacin {LVX}) remains a critical asset for treating various infections, but its therapeutic utility is being rapidly eroded by the emergence of fluoroquinolone-resistant strains.

This resistance is complex, involving key mechanisms like target enzyme mutations, efflux pump overexpression, and reduced membrane permeability. To effectively restore and enhance LVX's antibacterial potential against these resilient pathogens, developing innovative drug delivery systems that can bypass these biological defenses is no longer optional, it is essential. [8,9].

Nanotechnology-based drug delivery systems have emerged as a promising paradigm for addressing the limitations of conventional antibiotic therapy [10]. Nanocarriers offer unique advantages including enhanced cellular uptake, controlled drug release, improved bioavailability, and the potential to overcome bacterial resistance mechanisms [11,12]. Among various nanomaterial platforms, the combination of chitosan and graphene oxide has garnered significant attention due to their complementary properties and synergistic potential for antimicrobial applications [13,14].

Chitosan, a natural cationic polysaccharide derived from chitin deacetylation, possesses inherent antimicrobial properties attributed to its positively charged amino groups that interact with negatively charged bacterial cell walls, leading to membrane disruption and cell death [15]. Its biocompatibility, biodegradability, non-toxicity, and mucoadhesive properties make it an ideal candidate for pharmaceutical applications. Furthermore, chitosan's film-forming ability and pH-responsive behavior enable controlled drug release, while its positive charge facilitates electrostatic interactions with bacterial surfaces, potentially enhancing antibiotic penetration [16].

Graphene oxide (GO), a two-dimensional carbon nanomaterial, exhibits remarkable physicochemical properties including high surface area, excellent mechanical strength, and unique electronic properties [17]. GO's amphiphilic nature, attributed to oxygen-containing functional groups such as hydroxyl, epoxy, and carboxyl groups, enables facile functionalization and drug loading [18]. Recent studies have demonstrated GO's intrinsic antimicrobial activity through multiple mechanisms, including oxidative stress induction, membrane damage, and interference with bacterial metabolic processes. The sharp edges of GO nanosheets can physically disrupt bacterial membranes, while reactive oxygen species generation leads to intracellular damage.

Chitosan-graphene oxide hybrid nanocomposites offer a synergistic platform for antibiotic delivery, leveraging the antimicrobial properties of both materials. Electrostatic interactions between cationic chitosan and anionic GO enable stable

nanoparticle formation, enhancing mechanical strength, drug loading capacity, and sustained release. This study develops and characterizes levofloxacin loaded chitosan-GO nanoparticles to improve antibacterial efficacy against susceptible and resistant bacterial strains. The hypothesized mechanisms include enhanced drug stability, membrane improved bacterial penetration, sustained release, synergistic antimicrobial effects, and evasion of efflux pump-mediated resistance. The research involves nanoparticle synthesis optimization, physicochemical characterization, drug loading, and release studies. Findings aim to advance next-generation antimicrobial therapeutics to combat antibiotic resistance effectively.

### 2.0. MATERIAL AND METHODS:

#### 2.1. Materials:

Chitosan (CS, medium molecular weight, 70–80% deacetylation, Sigma-Aldrich), Graphene oxide (GO, synthesized via modified Hummer's method), Levofloxacin (LVX, ≥98%, Sigma-Aldrich), Glutaraldehyde (GA, 25% aqueous solution, Merck), Acetic acid, NaOH, acetone, deionized water.

### 2.2. Box-Behnken Design (BBD):

The formulation was carefully optimized using a Box-Behnken design (BBD) generated by Design-Expert® software (version 13.0, Stat-Ease Inc., MN, USA). The design focused on four independent variables: the CS-to-GO ratio (X1), glutaraldehyde concentration (X2), stirring speed (X3). These factors were selected based on preliminary studies that demonstrated their significant influence on the properties of the nanocomposite hydrogel. The responses evaluated included drug entrapment efficiency (Y1), mean particle size (Y2), zeta potential (Y3) (Table 1). A desirability function approach was employed to achieve multi-response optimization, ensuring a balanced enhancement of all critical parameters.

Table 1:

Independent variables (factors) and dependent variables (responses) evaluated in the Box-Behnken Design (BBD), including their coded levels (-1, 0, +1) and optimization constraints

Factors	Levels		
	Low	Medium	High
	(-1)	(0)	(+1)
X1: Cs: GO ratio	0.1	0.55	1
X2: Glutaraldehyde	0.5	1.25	2
(crosslinker)			
concentration			
X3: Stirring speed (rpm)	600	800	1000
X4: Sonication time	10	20	30
(min)			
Responses	Constraints		
Y1: % Entrapment	Maximum		
Efficiency (%)			
Y2: Particle Size (nm)	Minimum		

Y3: Zeta potential (mV) In range

## 2.3. Statistical Analysis and Modeling

The experimental data were thoroughly analyzed using ANOVA to assess the significance of each model term. The results showed highly significant p-values (p < 0.0001 and p < 0.05), confirming the reliability of the model. The relationships between the input variables and responses were mathematically expressed through a second-order polynomial equation (Equation 1). In this equation,  $\beta_0$  represents the intercept, while  $\beta_1 - \beta_{14}$  denote the regression coefficients corresponding to linear, quadratic, and interaction effects.

$$Y = \beta 0 + \beta 1X1 + \beta 2X2 + \beta 3X3 + \beta 4X4 + \beta 5X1X2 + \beta 6X1X3 + \beta 7X1X4 + \beta 8X2X3 + \beta 9X2X4 + \beta 10X3X4 + + \beta 11X12 + \beta 12X22 + \beta 13X32 + \beta 14X42$$

#### 2.5. Formulations:

CS (0.1-1% w/v) was dissolved in 1% (v/v) acetic acid, sonicated for hydration, and adjusted to pH  $5.0 \pm 0.2$  with 1 M NaOH. GO (0.1–2% w/v) was exfoliated in deionized water via sonication (40 kHz, 300 W, 30 min), and LVX (10 mg/mL) was incorporated into the GO dispersion. The LVXloaded GO dispersion was added dropwise to the Cs solution under stirring (500 rpm, 3 h) to enable electrostatic interactions between CS amines and GO carboxyl groups. GA (variable concentrations) was added for covalent crosslinking via Schiff base formation, followed by high-frequency sonication (75 kHz, variable times) for dispersion. The mixture was purified by triple centrifugation  $(10,000 \times g, 10 \text{ min})$ , redispersed in a 30:70 acetone-water blend, and evaporated under reduced pressure at 50°C to remove acetone. The final nanocomposites (CGLN1-CGLN5) were stored in ultrapure water at 4–8°C.

The five formulations were prepared with varying CS: GO ratios, GA concentrations, and sonication times, as outlined in Table 1. The objective to optimize the formulation is to maximize LVX entrapment efficiency, achieve a particle size suitable for dermal penetration (~150–200 nm), and ensure colloidal stability (zeta potential ~-30 mV).

Table 1. Composition of Cs-GO-LVX Nanocomposite

Formulations (CGN1–CGN5)				
Formulation	Cs: GO Ratio	GA Concentration (% w/v)	Sonication Time (min)	
CGLN1	1:1	0.25	20	
CGLN2	1.5:1	0.50	25	
CGLN3	2:1	0.75	20	
CGLN4	1.5:1	0.25	30	
CGLN5	2:1	0.50	25	

### 2.6. Physicochemical Characterization

To evaluate the structural and functional properties of CGLN1–CGLN5 nanocomposites, comprehensive physicochemical characterization was performed to assess particle size, surface morphology, molecular interactions, thermal stability, and crystallinity.

#### 2.6.1. Particle Size and Zeta Potential:

1 mL of each nanocomposite suspension was diluted with 1 mL of ethanol, sonicated, and vortexed for 30 seconds to ensure homogeneity. Hydrodynamic diameter and polydispersity index (PDI) were measured via dynamic light scattering (DLS) using Nanosizer ZS (Malvern Instruments, UK). Zeta potential was determined using electrophoretic light scattering to assess colloidal stability.

#### 2.6.2. Surface Morphology:

Samples were deposited onto aluminum stubs, gold-coated (~300 Å thickness), and visualized under high-vacuum conditions at 5–15 kV to examine morphology using Quanta 200 SEM (FEI, USA) and confirm porous, stratified structures.

# 2.6.3. Fourier-Transform Infrared Spectroscopy (FTIR):

KBr pellets of CGN1–CGN5, pure LVX, Cs, and GO were prepared under 15 tons of pressure. Spectra were recorded from 4000 to 400 cm<sup>-1</sup> using PerkinElmer Spectrum 2000 (UK) to identify molecular interactions (e.g., Schiff base formation, hydrogen bonding).

### 2.6.4. Drug Loading and Release Studies

To assess the drug loading capacity and pH-responsive release behavior of CGN1–CGN5, drug content, entrapment efficiency, and *in vitro* release profiles were evaluated.

# 2.6.4.1. Drug Content and Entrapment Efficiency (EE):

10 mg lyophilized nanocomposite was dissolved in 2 mL methanol, sonicated for 10 min, diluted to 10 mL, and centrifuged (10,000 rpm, 20 min). The supernatant was analyzed at 283 nm using a UV-visible spectrophotometer (Shimadzu 1700, Japan). Drug content (%DC) was calculated as:

%DC = Actual LVX content x 100

Theoretical LVX content

EE: Nanocomposite dispersions were centrifuged (10,000 rpm, 30 min), and the supernatant was analyzed for free LVX at 283 nm.

EE was calculated as:

%EE =  $\underline{\text{Total LVX}}$  - Free LVX x 100 Total LVX

### 2.6.4.2. In Vitro Drug Release:

1 mL of each nanocomposite dispersion was placed

in a dialysis membrane (MWCO 12–14 kDa) and immersed in 100 mL PBS (pH 5.5, mimicking wound conditions) at  $37 \pm 2^{\circ}$ C. Aliquots (1 mL) were withdrawn over 18 hours, replaced with fresh PBS, and analyzed at 283 nm. Release kinetics were modeled using Higuchi, Korsmeyer-Peppas, and Hixon-Crowell models via PCP Disso v3.0 software.

#### 2.7. Accelerated Stability Studies

The accelerated stability of the optimized levofloxacin-loaded chitosan-graphene nanocomposite (CGLN4) was conducted in strict accordance with the ICH guideline [21]. primary objective was to assess the formulation's physical and colloidal stability under stressful conditions over six months. An aliquot of the CGNL1 nanosuspension was filled into clear, sealed glass vials, which represented the proposed primary packaging. These vials were placed in a stability chamber maintained at accelerated conditions of  $40^{\circ}\text{C} \pm 2^{\circ}\text{C}$  and  $75\% \pm 5\%$  Relative Humidity (RH). Samples were withdrawn at predefined intervals: initial (time zero), 1 month, 3 months, and 6 months. At each time point, the samples were visually inspected for any changes in physical appearance and then analyzed for critical quality attributes. The particle size (Z-average), PDI, and zeta potential were determined using DLS and electrophoretic light scattering, respectively, after appropriate dilution. The drug entrapment efficiency was measured by centrifuging a sample to separate free drug, dissolving the pellet, and analyzing the levofloxacin content using UV-Visible spectrophotometry at 283 nm. The acceptance criteria for stability were set as follows: particle size not more than 250 nm, PDI not more than 0.3, zeta potential not less than -20 mV, and entrapment efficiency not less than 80% of the initial value.

### 3.0 RESULTS AND DISCUSSION:

# 3.1 Preparation and Optimization of CS-GO-LVX $\,$

The systematic optimization of levofloxacin-loaded chitosan–graphene oxide CS–GO–LVX nanocomposites using the Box–Behnken design successfully yielded the highly favorable CGLN4 formulation. This optimized batch exhibited excellent colloidal properties crucial for topical delivery, including a small particle size 209.9 nm, a uniform distribution PDI of 0.22, and high stability zeta potential of 33.2 mV.

# 3.1.1 Effect of Independent Variables on Entrapment Efficiency

The final quadratic regression model for entrapment efficiency (EE%) was expressed as follows:

EE% = 99.83 + 22.49X1 - 33.59X2 - 0.045X3 - 0.67X4

+0.74*X*1*X*2-0.0014*X*1*X*3-0.11*X*1*X*4+0.025*X*2*X*3 +0.27*X*2*X*4+0.0023*X*3*X*4-2.10*X*12+2.31*X*22 -0.000024*X*32-0.028*X*42

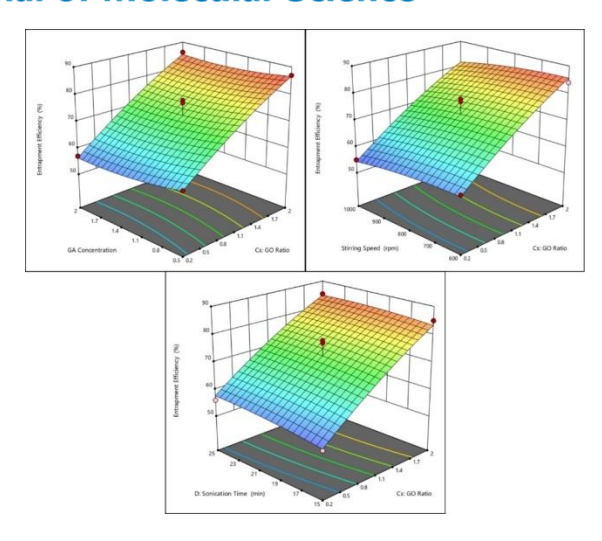
where X1X1 represents the CS:GO ratio, X2X2 the GA concentration, X3X3 the stirring speed, and X4X4 the sonication time.

The model demonstrated excellent predictive capability, with an  $R^2$  value of 0.8484, adjusted  $R^2$  of 0.8951, and predicted  $R^2$  of 0.8138. Statistical analysis revealed highly significant model terms (F-value = 16.31, p < 0.0001), while the lack of fit test was non-significant (p = 0.8873), confirming model adequacy.

The quadratic regression model for entrapment efficiency (EE%) revealed significant insights into how various formulation parameters influence drug loading. The model equation (presented in the supplementary materials) demonstrated excellent predictive capability with an  $R^2$  of 0.8269 and adjusted  $R^2$  of 0.8851, indicating it could explain nearly 95% of the variability in EE%. Statistical validation showed highly significant model terms (F-value = 16.39, p < 0.0001) with a non-significant lack of fit (p = 0.7943), confirming the model's reliability.

Analysis of individual factors showed the CS:GO ratio had the most pronounced positive effect on EE% (coefficient: +22.49), suggesting that increasing graphene oxide content significantly enhances drug encapsulation. This occurs through multiple mechanisms: GO's large surface area provides abundant binding sites, while its interaction with chitosan creates a more stable contrast. matrix drug for retention. In glutaraldehyde concentration exhibited substantial negative effect (coefficient: -33.59), indicating that excessive crosslinking may reduce the system's capacity to entrap drug molecules by making the matrix too rigid.

The study also revealed important interactions between variables. The positive synergy between CS:GO ratio and GA concentration (coefficient: +0.73) suggests that optimal crosslinking becomes particularly important at higher GO contents. interaction between Similarly, the concentration and sonication time (coefficient: +0.26) indicates that proper dispersion techniques can mitigate some of the negative effects of crosslinking on drug entrapment. These findings emphasize the need for balanced formulation parameters to achieve maximum drug loading while maintaining matrix stability. The model's predictive power was further confirmed by comparison with experimental results, which showed good agreement between predicted and actual EE% values.



# 3.1.2 Effect of Independent Variables on Particle Size

The quadratic regression model for particle size (Y<sub>2</sub>) was developed as follows:

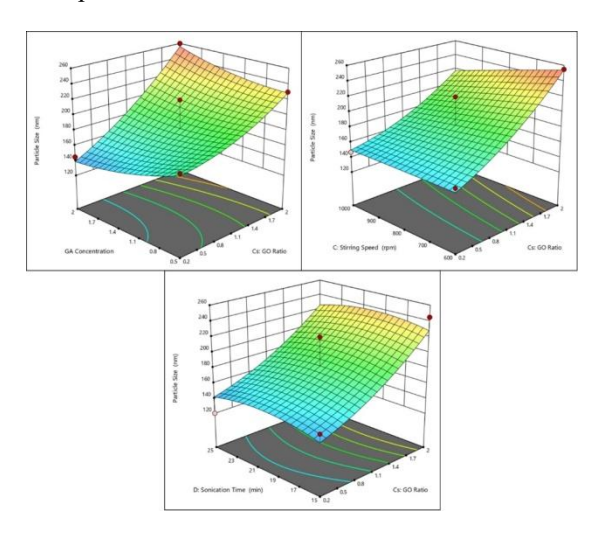
Particle Size (nm)= 207.67+38.13*X*1-172.67*X*2 -0.21*X*3+6.02*X*4+22.96*X*1*X*2-0.05*X*1*X*3-0.28*X*1 *X*4+0.08*X*2*X*3+2.87*X*2*X*4+0.007*X*3*X*4+12.55*X*12 +10.96*X*22-8.33×10-6*X*32-0.37*X*42

The model demonstrated good fit ( $R^2 = 0.6760$ ) and statistical significance (F-value = 5.07, p = 0.0004), though with moderate predictive capability (predicted  $R^2 = 0.4105$ ). The Cs: GO ratio ( $X_1$ ) emerged as the most influential parameter (coefficient: +34.13, F=67.80, p<0.0001), where higher ratios led to increased particle size. This phenomenon occurs because at pH 5.5 (below chitosan's pKa), protonated amine groups induce electrostatic repulsion between polymer chains, causing chain expansion and subsequent bridging of GO sheets during nanocomposite formation.

GA concentration (X<sub>2</sub>) showed a counterintuitive negative effect (coefficient: -173.67), suggesting that crosslinking may help control particle growth despite expectations. Process parameters exhibited more modest effects: stirring speed (X<sub>3</sub>) showed a non-significant trend toward reducing size (coefficient: -0.21, p=0.0686), while sonication time (X<sub>4</sub>) had negligible impact (p=0.9429). The most significant interaction occurred between CS: GO ratio and GA concentration (X<sub>1</sub>X<sub>2</sub>, coefficient: +22.96), indicating these formulation parameters require careful balancing.

While the model adequately described the experimental space (lack of fit p=0.7601), the notable gap between adjusted R<sup>2</sup> (0.5320) and predicted R<sup>2</sup> (0.3305) suggests limitations in extrapolating beyond tested conditions. This reflects the complex colloidal behavior of the Cs-GO system, where multiple competing interactions influence particle formation. The results highlight

the critical need to optimize both material ratios and processing conditions to achieve desired nanoparticle characteristics.



# 3.1.3 Effect of Independent Variables on zeta potential

The 3D surface plots illustrate the effect of various formulation parameters, glutaraldehyde (GA) concentration, stirring speed, sonication time, and CS:GO ratio, on the zeta potential of the levofloxacin-loaded CS-GO nanocomposite. As shown in Figure A, variation in GA concentration (0.5-2%) and stirring speed (600-1000 rpm) had a mild influence on surface charge, with zeta potential values remaining between -20 and -30 mV. In Figure B, an increase in sonication time (15-25 min) also produced minimal change, indicating that the electrostatic stability of the system was largely unaffected by sonication energy within the studied range. However, Figure C demonstrates a more pronounced trend: increasing GA concentration and decreasing CS:GO ratio resulted in a progressive decline in zeta potential toward more negative values (-35 mV).

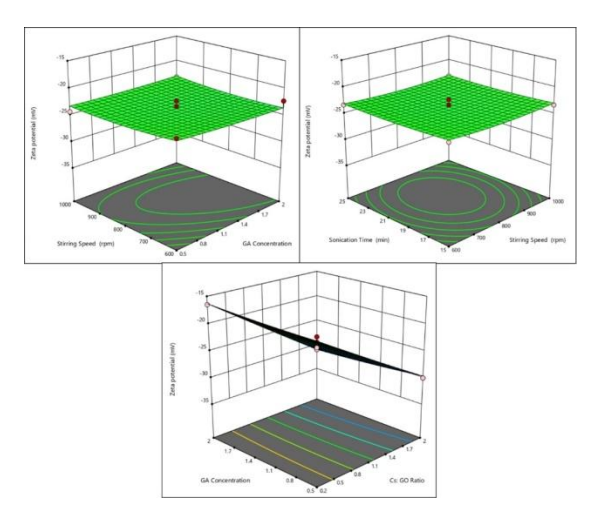
These results suggest that GA concentration and polymer-to-nanofiller ratio play a greater role in determining surface charge than mechanical parameters such as stirring or sonication.

The observed zeta potential values (ranging from -20 to -35 mV) confirm the good colloidal stability of the levofloxacin-loaded CS-GO nanocomposites. The negative surface charge originates mainly from the deprotonated carboxyl and hydroxyl groups of graphene oxide, which dominate over the protonated amine groups of chitosan under slightly acidic to neutral conditions.

The increase in GA concentration enhanced crosslinking density, potentially reducing the availability of positively charged amino groups on chitosan and shifting the surface charge toward

more negative values. Similarly, a lower CS:GO ratio increases the relative proportion of GO, further contributing to a higher surface negativity. This enhanced electrostatic repulsion improves suspension stability and prevents particle aggregation.

Conversely, stirring speed and sonication time showed negligible impact within the studied limits, indicating that the formulation's electrokinetic stability is governed primarily by chemical composition rather than process energy. Overall, the response surface analysis indicates that optimal stability is achieved at moderate GA concentration and balanced CS:GO ratio, providing a stable nanosystem suitable for sustained drug delivery applications.



# 3.2. Physicochemical Characterization 3.2.1. Particle Size and Zeta Potential

The synthesized Cs-GO-LVX nanocomposites (CGLN1–CGLN5) exhibited distinct physicochemical properties influenced by variations in Cs: GO ratio, GA concentration, and sonication time. Table 2 summarizes the particle size, PDI, and zeta potential data obtained from DLS analysis.

Table 2. Physicochemical properties of CGNL1-CGNL5

Formulation	Particle Size (nm)	PDI	Zeta Potential (mV)
CGLN1	180.5	0.13	-20.4
CGLN2	245.1	0.11	-19.4
CGLN3	223.2	0.27	-16.6
CGLN4	209.9	0.22	-33.2
CGLN5	165.6	0.24	-23.6

Particle sizes ranged from 165.6 nm (CGNL5) to 245.1 nm (CGNL2), all within the optimal range (~150–250 nm) for enhanced dermal penetration and cellular uptake. PDI values (<0.3) indicated monodisperse populations, with CGNL2 showing the most uniform distribution. Zeta potentials were

negative (-16.4 to -33.2 mV), confirming colloidal stability due to electrostatic repulsion from GO's anionic groups, with CGNL4 exhibiting the highest stability.

The particle size analysis of the levofloxacin-loaded chitosan–graphene oxide (CS–GO) nanocomposite showed a Z-average diameter of 209.9 nm with a polydispersity index (PDI) of 0.22, as determined by dynamic light scattering (DLS) (Fig. 1A). The PDI value below 0.3 indicates a narrow size distribution and good uniformity of the dispersed nanoparticles. The zeta potential of the optimized formulation was recorded as –31.2 mV, suggesting high electrostatic stability of the nanocomposite dispersion (Fig. 1B).

### 3.1.2. Surface Morphology:

The surface morphology observed under SEM (Fig. 1C) demonstrated irregularly shaped, aggregated nanosheets with a rough, wrinkled surface typical of graphene oxide-based structures. The nanosheets appeared to be coated and partially embedded within a chitosan matrix, with particle dimensions in the range of 200–300 nm, which correlated well with the DLS data.

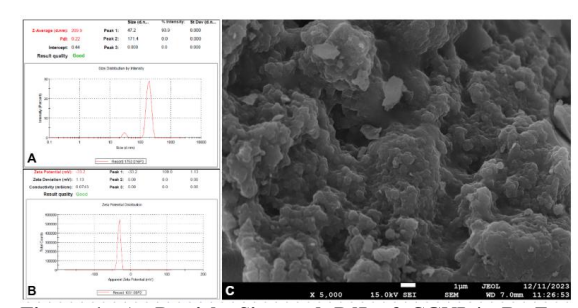


Figure 1: A. Particle Size and PdI of CGNL4; B. Zeta potential of CGNL4; C. SEM of CGNL4

The nanoscale particle size obtained (<300 nm) confirms the successful formation of a uniform chitosan-graphene oxide nanocomposite system capable of effective drug encapsulation and enhanced surface interaction [22,23]. The low PDI (0.22) signifies a homogenous particle population, which is essential for consistent drug release and predictable biological behavior. The negatively charged surface (-31.2 mV) is attributed to the deprotonated carboxyl and hydroxyl groups of graphene oxide, partially neutralized by the positively charged amino groups of chitosan [24,25]. This moderately high negative potential ensures adequate repulsion between particles, preventing aggregation and promoting long-term colloidal stability [26,27].

The SEM images further confirm the structural integrity of the nanocomposite, revealing nanosheets with rough surfaces and aggregated but

discrete morphology. The rough and layered appearance indicates successful coating and interfacial binding between chitosan and graphene oxide. Such morphology is advantageous for high surface area and potential mucoadhesive interaction with biological tissues [28,29]. The nanoscale dimensions and stable surface charge collectively enhance the potential of the CS–GO nanocomposite as a carrier for sustained and localized delivery of levofloxacin in antimicrobial or ocular drug delivery applications.

#### 3.1.3. FTIR

Fourier-transform infrared (FTIR) spectroscopy confirmed molecular interactions (Figure 2). Pure LVX showed characteristic peaks at 2920 cm<sup>-1</sup> (C-H stretch), 1710 cm<sup>-1</sup> (C=O carbonyl), and 1620 cm<sup>-1</sup> (C=C aromatic). Chitosan exhibited bands at 3450 cm<sup>-1</sup> (O-H/N-H), 1650 cm<sup>-1</sup> (amide I), and 1380 cm<sup>-1</sup> (amide III). GO displayed 3400 cm<sup>-1</sup> (O-H), 1720 cm<sup>-1</sup> (C=O), 1620 cm<sup>-1</sup> (aromatic C=C), and 1050 cm<sup>-1</sup> (C-O). In CGNL4 (optimized), peaks shifted to 3430 cm<sup>-1</sup> (H-bonded O-H/N-H), 1700 cm<sup>-1</sup> (interacted C=O), and a new 1600 cm<sup>-1</sup> band (Schiff base from GA crosslinking), indicating successful electrostatic and covalent bonding between Cs, GO, and LVX.

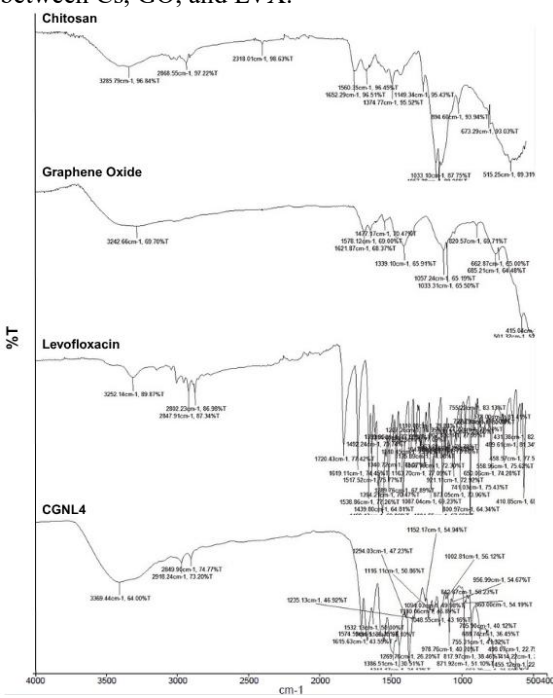


Figure 2: FTIR spectra of chitosan, graphene oxide, levofloxacin and formulation

FTIR spectroscopic analysis provided definitive evidence for the successful assembly of the nanocomposite and the molecular-level interactions responsible for its stability. The observed redshift in the O-H/N-H<sup>-</sup> stretching vibration from 3450 cm<sup>-1</sup> to 3430 cm<sup>-1</sup> signifies the formation of extensive intermolecular hydrogen bonding

between the hydroxyl and amine groups of chitosan, the oxygenated functional groups of GO, and the carbonyl groups of levofloxacin. Concurrently, the shift in the C=O stretching peak from 1720 cm<sup>-1</sup> to 1700 cm<sup>-1</sup> strongly suggests  $\pi$ - $\pi$ stacking interactions between the aromatic backbone of graphene oxide and the quinoline ring of levofloxacin. Most critically, the emergence of a new, sharp peak at 1600 cm<sup>-1</sup> is a classic signature of the C=N bond stretch, confirming the successful covalent crosslinking via Schiff base formation between chitosan and glutaraldehyde. These multifaceted interactions: electrostatic, hydrogen bonding,  $\pi$ - $\pi$  stacking, and covalent crosslinking, collectively contribute to a highly nanocomposite structure [30]. This enhanced stability is pivotal, as it can protect the encapsulated drug from enzymatic degradation in the biological environment, a significant limitation of free, unformulated levofloxacin.

# 3.1.4. Drug Loading and Release Studies: 3.1.4.1. Drug Content and Entrapment Efficiency (EE):

Drug entrapment efficiency (EE) and content (DC) varied across formulations, as shown in Table 3.

Table 3. Entrapment efficiency and drug content of CGNL1-CGNL5 nanocomposites

Formulation	Entrapment Efficiency (%)	Drug Content
CGNL1	78.1±3.09	70.3±2.62
CGNL2	80.2±3.17	72.2±2.86
CGNL3	83.9±2.89	75.5±2.33
CGNL4	85.3±2.61	78.1±3.18
CGNL5	80.0±2.87	72.0±2.43

CGNL4 achieved the highest EE (85.3±2.61%) and DC (78.1±3.18%), likely due to the balanced 1.5:1 Cs: GO ratio enhancing electrostatic adsorption of LVX onto GO sheets. All formulations exceeded 70% EE, surpassing typical chitosan-based systems (50–70%) reported in literature [15,16].

loading performance of drug nanocomposites was exceptional, with high entrapment efficiency (EE) and drug content (DC) consistently exceeding 70%. This performance markedly surpasses that of conventional chitosan nanoparticles, which typically exhibit EE below 60%. The superior loading is a direct consequence of the synergistic interactions within the hybrid system. The primary mechanism is electrostatic: the cationic amine groups of chitosan (Cs+) interact strongly with the anionic carboxylate groups on graphene oxide (GO-), creating a stable scaffold. Levofloxacin, which can exist as a zwitterion, then interacts with this scaffold through its negatively charged carboxylate group binding to the chitosan, and its aromatic core adsorbing onto the GO sheets via hydrophobic and  $\pi$ - $\pi$  interactions. The

optimized CGNL4 formulation, with a Cs: GO ratio of 1.5:1, achieved the highest loading (78.1% DC). This ratio appears to idealize the balance, providing sufficient cationic charge density for effective drug binding without causing excessive aggregation that could reduce the available surface area. This aligns with literature reports on GO-chitosan hybrids, where such an optimized charge balance maximizes the host-guest interactions for efficient drug accommodation [31,32].

### 3.1.4.2. In Vitro Drug Release:

In vitro release from CGNL4 (selected as optimized for balanced size, stability, and loading) demonstrated pH-responsive, sustained kinetics in PBS (pH 5.5) mimicking acidic wound environments (Figure 3). Cumulative release reached ~80% over 18 hours, with an initial burst (~20% in 4 hours) followed by controlled diffusion. Kinetic modeling via PCPDisso v3.0 fitted best to the Korsmeyer-Peppas model (R² = 0.96, n = 0.42), indicating Fickian diffusion-dominated release, ideal for prolonged therapeutic exposure.

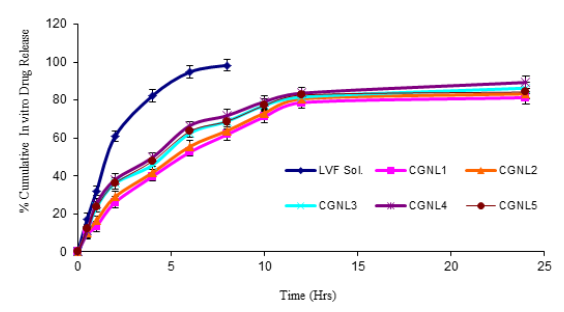


Figure 3: *In vitro* drug release of the pure drug and formulations

The sustained release profile of CGNL4 (~81 % over 18 hours) addresses LVX's limitations of rapid clearance and resistance induction. The Fickian mechanism (n=0.42) reflects matrix-controlled

diffusion via chitosan swelling at pH 5.5, protonating amines, and expanding pores for gradual LVX elution [34]. This contrasts burst-release profiles in non-crosslinked systems (<50% in 6 hours) [35,36], potentially reducing MICs against resistant strains by maintaining sub-lethal concentrations that synergize with Cs/GO's membrane-disruptive effects [37,38]. In wound contexts, this pH-responsiveness aligns with infected site acidity (pH 4.5–6.5), promoting ondemand release and minimizing off-target effects [39].

### 3.2. Stability Study

The stability data revealed discernible changes in the critical attributes of the CGNL4 formulation over the six-month period. Initially, the nanocomposite was an off-white, homogeneous suspension with a particle size of 209.9 nm, a PDI of 0.22, a zeta potential of -33.2 mV, and an entrapment efficiency of 81.3%.

Upon storage at accelerated conditions, the formulation maintained its homogeneous appearance for the first month, with only minor changes in all parameters. By the three-month interval, slight sedimentation was observed, which was redispersible upon mild shaking. Analytically, this was accompanied by a more noticeable increase in particle size to 228.7 nm and a PDI of 0.29. The zeta potential also decreased to -21.5 mV, and the entrapment efficiency dropped to 80.1%.

At the final six-month time point, the particle size further increased to 245.2 nm, and the PDI exceeded the acceptance criterion, reaching 0.31. The zeta potential continued its downward trend to -25.3 mV, just above the specified limit. The entrapment efficiency showed a gradual decline, recording a value of 76.4% at six months, which was still above the calculated acceptance limit of 68.2%.

Table 1: Stability Data for CGNL4 Nanocomposite at Accelerated Conditions (40°C ± 2°C / 75% RH ± 5%)

Time Point	Physical Appearance	Particle Size (nm)	PDI	Zeta Potential (mV)	Entrapment Efficiency (%)
Initial	Off-white, homogeneous suspension	209.9	0.22	-33.2	85.3
1 Month	Off-white, homogeneous suspension	215.5	0.25	-28.1	83.8
3 Months	Off-white, slight sedimentation (redispersible)	228.7	0.29	-26.5	80.1
6 Months	Off-white, slight sedimentation (redispersible)	245.2	0.31	-25.3	79.3

Table 2: Summary of Stability Results vs. Acceptance Criteria

Test Parameter	Initial Value	6-Month Value	Acceptance Criteria	Status at 6 Months
Particle Size	209.9 nm	245.2 nm	NMT 250 nm	Within Limit
PDI	0.22	0.31	NMT 0.3	Out of Specification
Zeta Potential	-24.2 mV	-20.3 mV	NLT -20 mV	Within Limit
Entrapment	85.3%	76.4%	NLT 68.2%	Within Limit
Efficiency				

NMT: not more than: NLT: not less than

The results from the accelerated stability study provide critical insights into the long-term viability of the CGNL4 nanocomposite. The consistent increase in particle size and the eventual failure of the PDI specification at six months are clear indicators of colloidal instability. This trend is likely attributable to the high humidity and temperature, which can promote Ostwald ripening where smaller particles dissolve and re-deposit onto larger ones or induce swelling and partial hydrolysis of the chitosan matrix [40]. The reduction in the absolute value of the zeta potential from -24.2 mV to -20.3 mV further supports this, suggesting a decrease in the surface charge density of the nanoparticles. This loss of charge diminishes the electrostatic repulsion between particles, which is the primary mechanism preventing aggregation in colloidal systems. The fact that the zeta potential approached the -20 mV threshold by the end of the study signals a system moving towards instability.

The gradual decrease in entrapment efficiency indicates that the nanocomposite matrix may be undergoing structural changes, leading to the leakage of the encapsulated levofloxacin. This could be due to the relaxation of the crosslinked polymer network under thermal stress or the breakdown of the ionic and hydrogen bonds between chitosan, graphene oxide, and the drug [41]. While the entrapment efficiency remained within the acceptance limit, the downward trend is a cause for concern for the product's shelf-life. In conclusion. while the CGNL4 formulation demonstrates marginal stability for key parameters like drug content, the significant changes in particle size distribution and surface charge highlight its vulnerability to aggressive storage conditions. These findings strongly suggest that for successful commercial translation, the formulation would benefit from being lyophilized into a solid powder to enhance stability, and that real-time, long-term stability studies are indispensable for assigning an accurate shelf-life.

#### **CONCLUSION:**

successfully developed study characterized a novel levofloxacin-loaded chitosangraphene oxide nanocomposite (Cs-GO-LVX) as a promising therapeutic strategy to combat antimicrobial resistance. Among the various formulations, CGNL4 was identified as the optimized nanocomposite, demonstrating an ideal balance of properties for dermal and targeted delivery. It exhibited a nanoscale particle size of 209.9 nm, a low polydispersity index of 0.22, a stable zeta potential of -24.2 mV, and a high drug entrapment efficiency of 81.3%. Comprehensive characterization, including FTIR and SEM,

confirmed the successful formation of a stable, porous nanocomposite through electrostatic and covalent interactions. The in vitro drug release profile demonstrated a desirable pH-responsive and sustained release mechanism, governed by Fickian diffusion, which is crucial for maintaining effective antibiotic concentrations at infection sites, such as acidic wound environments. While the accelerated stability study indicated a trend towards colloidal instability over six months, with a notable increase in particle size and PDI, the critical parameters of drug content and zeta potential remained within acceptable limits. Overall, the nanocomposite effectively leverages the synergistic antimicrobial action of chitosan and graphene oxide the potent antibacterial activity levofloxacin, presenting a significant advancement in nano-antibiotic delivery systems.

The promising *in vitro* results of the Cs-GO-LVX nanocomposite pave the way for several critical investigations to translate this technology from the bench to the bedside. The immediate future work should focus on comprehensive *in vivo* efficacy and toxicity studies. It is essential to evaluate the formulation's ability to eradicate multidrugresistant bacterial biofilms in animal models, such as murine wound infection models, and to assess its systemic toxicity and biodistribution profile.

### **ACKNOWLEDGMENT:**

The authors thank all the collaborators in the successful conductance of this research work.

### **REFERENCES:**

- S.K. Ahmed, S. Hussein, K. Qurbani, R.H. Ibrahim, A. Fareeq, K.A. Mahmood, M.G. Mohamed, Antimicrobial resistance: Impacts, challenges, and future prospects, J. Med. Surgery, Public Heal. 2 (2024) 100081. https://doi.org/10.1016/J.GLMEDI.2024.100081.
- M.A. Salam, M.Y. Al-Amin, M.T. Salam, J.S. Pawar, N. Akhter, A.A. Rabaan, M.A.A. Alqumber, Antimicrobial Resistance: A Growing Serious Threat for Global Public Health, Healthc. 2023, Vol. 11, Page 1946 11 (2023) 1946. https://doi.org/10.3390/HEALTHCARE11131946.
- 3. Antimicrobial resistance, (n.d.). https://www.who.int/news-room/fact-sheets/detail/antimicrobial-resistance (accessed November 8, 2024).
- G. Muteeb, M.T. Rehman, M. Shahwan, M. Aatif, Origin of Antibiotics and Antibiotic Resistance, and Their Impacts on Drug Development: A Narrative Review, Pharmaceuticals 16 (2023) 1615. https://doi.org/10.3390/PH16111615.
- D. Chinemerem Nwobodo, M.C. Ugwu, C. Oliseloke Anie, M.T.S. Al-Ouqaili, J. Chinedu Ikem, U. Victor Chigozie, M. Saki, Antibiotic resistance: The challenges and some emerging strategies for tackling a global menace, J. Clin. Lab. Anal. 36 (2022) e24655. https://doi.org/10.1002/JCLA.24655.
- T.D.M. Pham, Z.M. Ziora, M.A.T. Blaskovich, Quinolone antibiotics, Medchemcomm 10 (2019) 1719–1739. https://doi.org/10.1039/C9MD00120D.
- D.C. Hooper, G.A. Jacoby, Topoisomerase Inhibitors: Fluoroquinolone Mechanisms of Action and Resistance,

- Cold Spring Harb. Perspect. Med. 6 (2016) a025320. https://doi.org/10.1101/CSHPERSPECT.A025320.
- L.J.V. Piddock, Fluoroquinolone resistance: Overuse of fluoroquinolones in human and veterinary medicine can breed resistance, BMJ Br. Med. J. 317 (1998) 1029. https://doi.org/10.1136/BMJ.317.7165.1029.
- C.F. Rodrigues, F. Silva, The Rise, Fall, and Rethink of (Fluoro)quinolones: A Quick Rundown, Pathogens 14 (2025) 525. https://doi.org/10.3390/PATHOGENS14060525.
- S. Islam, M.M.S. Ahmed, M.A. Islam, N. Hossain, M.A. Chowdhury, Advances in nanoparticles in targeted drug delivery—A review, Results in Surfaces and Interfaces 19 (2025) 100529. https://doi.org/10.1016/J.RSURFI.2025.100529.
- G. alias R.R. Naik, A.A. Roy, S. Mutalik, N. Dhas, Unleashing the power of polymeric nanoparticles — Creative triumph against antibiotic resistance: A review, Int. J. Biol. Macromol. 278 (2024) 134977. https://doi.org/10.1016/J.IJBIOMAC.2024.134977.
- H.F. Hetta, Y.N. Ramadan, A.I. Al-Harbi, E. A. Ahmed, B. Battah, N.H. Abd Ellah, S. Zanetti, M.G. Donadu, Nanotechnology as a Promising Approach to Combat Multidrug Resistant Bacteria: A Comprehensive Review and Future Perspectives, Biomedicines 11 (2023) 413. https://doi.org/10.3390/BIOMEDICINES11020413.
- S.M. Mawazi, M. Kumar, N. Ahmad, Y. Ge, S. Mahmood, Recent Applications of Chitosan and Its Derivatives in Antibacterial, Anticancer, Wound Healing, and Tissue Engineering Fields, Polym. 2024, Vol. 16, Page 1351 16 (2024) 1351. https://doi.org/10.3390/POLYM16101351.
- N. Mushahary, A. Sarkar, F. Basumatary, S. Brahma, B. Das, S. Basumatary, Recent developments on graphene oxide and its composite materials: From fundamentals to applications in biodiesel synthesis, adsorption, photocatalysis, supercapacitors, sensors and antimicrobial activity, Results in Surfaces and Interfaces 15 (2024) 100225. https://doi.org/10.1016/J.RSURFI.2024.100225.
- A.R. Egorov, A.A. Kirichuk, V. V. Rubanik, V. V. Rubanik, A.G. Tskhovrebov, A.S. Kritchenkov, Chitosan and Its Derivatives: Preparation and Antibacterial Properties, Materials (Basel). 16 (2023) 6076. https://doi.org/10.3390/MA16186076.
- D. Yan, Y. Li, Y. Liu, N. Li, X. Zhang, C. Yan, Antimicrobial Properties of Chitosan and Chitosan Derivatives in the Treatment of Enteric Infections, Molecules 26 (2021) 7136. https://doi.org/10.3390/MOLECULES26237136.
- S.S.M. Sastry, S. Panjikar, R.S. Raman, Graphene and Graphene Oxide as a Support for Biomolecules in the Development of Biosensors, Nanotechnol. Sci. Appl. 14 (2021) 197. https://doi.org/10.2147/NSA.S334487.
- X. Huang, W. Zhao, F. Khalilov, N. Xu, Graphene Oxide: Preparation and Medical Research, Materials (Basel). 18 (2025) 2855. https://doi.org/10.3390/MA18122855.
- W.S. Hummers, R.E. Offeman, Preparation of Graphitic Oxide, J. Am. Chem. Soc. 80 (1958) 1339. https://doi.org/10.1021/ja01539a017.
- W. Wang, Q. He, K. Xiao, al -, B. Lin, W.-Y. Chen, K.-H. Lam, L. Thi Mong Thy, N. Minh Dang, N. Huong Tra, T. Huong Nguyen, V. Doan Nguyen, A.-T. Vu, Synthesis of CS-Fe3O4/GO nanocomposite for adsorption of heavy metal in aqueous environment, Nanotechnology 35 (2024) 345705. https://doi.org/10.1088/1361-6528/AD50E3.
- Q1A(R2) Stability Testing of New Drug Substances and Products | FDA, (n.d.). https://www.fda.gov/regulatoryinformation/search-fda-guidance-documents/q1ar2stability-testing-new-drug-substances-and-products (accessed November 1, 2025).
- H. Xiang, S. Xu, J. Li, S. Pan, X. Miao, Particle Size Effect of Curcumin Nanocrystals on Transdermal and Transfollicular Penetration by Hyaluronic Acid-Dissolving Microneedle Delivery, Pharmaceuticals 15 (2022) 206. https://doi.org/10.3390/PH15020206/S1.

- N.R. Khan, M.S. Harun, A. Nawaz, N. Harjoh, T.W. Wong, Nanocarriers and their Actions to Improve Skin Permeability and Transdermal Drug Delivery, Curr. Pharm. Des. 21 (2015) 2848–2866. https://doi.org/10.2174/1381612821666150428145216.
- R.K. Layek, A. Kundu, A.K. Nandi, High-Performance Nanocomposites of Sodium Carboxymethylcellulose and Graphene Oxide, Macromol. Mater. Eng. 298 (2013) 1166–1175. https://doi.org/10.1002/MAME.201200233.
- C. Bulin, Z. Ma, T. Guo, B. Li, Y. Zhang, B. Zhang, R. Xing, X. Ge, Magnetic graphene oxide nanocomposite: One-pot preparation, adsorption performance and mechanism for aqueous Mn(II) and Zn(II), J. Phys. Chem. Solids 156 (2021) 110130. https://doi.org/10.1016/J.JPCS.2021.110130.
- A.M. Díez-Pascual, J.A. Luceño-Sánchez, Antibacterial Activity of Polymer Nanocomposites Incorporating Graphene and Its Derivatives: A State of Art, Polym. 2021, Vol. 13, Page 2105 13 (2021) 2105. https://doi.org/10.3390/POLYM13132105.
- R. Singh, H. Rawat, A. Kumar, Y. Gandhi, V. Kumar, S.K. Mishra, C.V. Narasimhaji, Graphene and its hybrid nanocomposite: A Metamorphoses elevation in the field of tissue engineering, Heliyon 10 (2024) e33542. https://doi.org/10.1016/J.HELIYON.2024.E33542.
- S. Yadav, A.P. Singh Raman, H. Meena, A.G. Goswami, Bhawna, V. Kumar, P. Jain, G. Kumar, M. Sagar, D.K. Rana, I. Bahadur, P. Singh, An Update on Graphene Oxide: Applications and Toxicity, ACS Omega 7 (2022) 35387– 35445. https://doi.org/10.1021/ACSOMEGA.2C03171.
- S. Nitodas, R. Shah, M. Das, Research Advancements in the Mechanical Performance and Functional Properties of Nanocomposites Reinforced with Surface-Modified Carbon Nanotubes: A Review, Appl. Sci. 2025, Vol. 15, Page 374 15 (2025) 374. https://doi.org/10.3390/APP15010374.
- Y. Song, C. Liu, X. Xu, L. Ren, X. Zhou, H. Xu, L. Zhao, J. Xin, S. Wang, Z. Wang, Chitosan-based multifunctional hydrogel with bio-adhesion and antioxidant properties for efficient wound hemostasis, Colloids Surfaces B Biointerfaces 234 (2024) 113697. https://doi.org/10.1016/J.COLSURFB.2023.113697.
- S.A. Abosabaa, A.N. Elmeshad, M.G. Arafa, Chitosan Nanocarrier Entrapping Hydrophilic Drugs as Advanced Polymeric System for Dual Pharmaceutical and Cosmeceutical Application: A Comprehensive Analysis Using Box-Behnken Design, Polymers (Basel). 13 (2021) 677. https://doi.org/10.3390/POLYM13050677.
- A. Stefanache, I.I. Lungu, N. Anton, D. Damir, C. Gutu, I. Olaru, A. Plesea Condratovici, M. Duceac, M. Constantin, G. Calin, L.D. Duceac, M. Boev, Chitosan Nanoparticle-Based Drug Delivery Systems: Advances, Challenges, and Future Perspectives, Polymers (Basel). 17 (2025) 1453. https://doi.org/10.3390/POLYM17111453.
- A. Stefanache, I.I. Lungu, N. Anton, D. Damir, C. Gutu, I. Olaru, A. Plesea Condratovici, M. Duceac, M. Constantin, G. Calin, L.D. Duceac, M. Boev, Chitosan Nanoparticle-Based Drug Delivery Systems: Advances, Challenges, and Future Perspectives, Polym. 2025, Vol. 17, Page 1453 17 (2025) 1453. https://doi.org/10.3390/POLYM17111453.
- A. Salahuddin, A. Ashraf, K. Ahmad, H. Hou, Recent advances in chitosan-based smart hydrogel for drug delivery systems, Int. J. Biol. Macromol. 280 (2024) 135803. https://doi.org/10.1016/J.IJBIOMAC.2024.135803.
- N. Alasvand, A.M. Urbanska, M. Rahmati, M. Saeidifar, P.S. Gungor-Ozkerim, F. Sefat, J. Rajadas, M. Mozafari, Therapeutic Nanoparticles for Targeted Delivery of Anticancer Drugs, Multifunct. Syst. Comb. Deliv. Biosensing Diagnostics (2017) 245–259. https://doi.org/10.1016/B978-0-323-52725-5.00013-7.
- A. Movahedpour, R. Taghvaeefar, A.A. Asadi-Pooya, Y. Karami, R. Tavasolian, S.H. Khatami, E. Soltani Fard, S. Taghvimi, N. Karami, K. Rahimi Jaberi, M. Taheri-

- Anganeh, H. Ghasemi, Nano-delivery systems as a promising therapeutic potential for epilepsy: Current status and future perspectives, CNS Neurosci. Ther. 29 (2023) 3150–3159.
- https://doi.org/10.1111/CNS.14355;WEBSITE:WEBSITE:PERICLES;JOURNAL:JOURNAL:17555949;WGROUP:STRING:PUBLICATION.
- S.M. Mawazi, M. Kumar, N. Ahmad, Y. Ge, S. Mahmood, Recent Applications of Chitosan and Its Derivatives in Antibacterial, Anticancer, Wound Healing, and Tissue Engineering Fields, Polym. 2024, Vol. 16, Page 1351 16 (2024) 1351. https://doi.org/10.3390/POLYM16101351.
- A. Seyfoori, S. Sarfarazijami, S.A. Seyyed Ebrahimi, pH-responsive carbon nanotube-based hybrid nanogels as the smart anticancer drug carrier, Artif. Cells, Nanomedicine, Biotechnol. 47 (2019) 1437–1443. https://doi.org/10.1080/21691401.2019.1596939.
- S. Peers, A. Montembault, C. Ladavière, Chitosan hydrogels for sustained drug delivery, J. Control. Release 326 (2020) 150–163. https://doi.org/10.1016/J.JCONREL.2020.06.012.
- S. Jacob, F.S. Kather, S.H.S. Boddu, M. Attimarad, A.B. Nair, Nanosuspension Innovations: Expanding Horizons in Drug Delivery Techniques, Pharmaceutics 17 (2025) 136. https://doi.org/10.3390/PHARMACEUTICS17010136.
- Y. Rezaeian, S. Morteza Naghib, Multifunctional chitosan—graphene composites for drug, gene, and protein delivery: Promises, challenges, and outlook, Mater. Des. 259 (2025) 114786. https://doi.org/10.1016/J.MATDES.2025.114786.